IEEE Access
Multidisciplinary | Rapid Review | Open Access Journal

Received 3 October 2022, accepted 23 October 2022, date of publication 1 November 2022, date of current version 8 November 2022.

Digital Object Identifier 10.1109/ACCESS.2022.3218673

RESEARCH ARTICLE

Circular Formation Guidance of Fixed-Wing UAVs Using Mesh Network

SUHYEON KIM, HYEONGJUN CHO, AND DONGWON JUNG, (Member, IEEE)
Department of Smart Drone Convergence, Korea Aerospace University, Goyang-si 10540, South Korea

Corresponding author: Dongwon Jung (djung@kau.ac.kr)

This work was supported in part by the National Research Foundation of Korea (NRF) funded by the Korean Government [Ministry of Science and ICT (MSIT)], in 2021, under Project 2021K1A3A1A49097955; and in part by the Vision-Based Robust Cooperative Multiple Target Tracking by a Decentralized Formation of Unmanned Aerial Vehicles (UAVs).

ABSTRACT This paper presents the guidance algorithm for the circular formation flight of multiple fixed-wing UAVs. The formation guidance law aims at reducing both the radial and the phase angle error with respect to the moving reference point located at a fixed distance from the leader UAV. To this end, the proposed guidance law generates the desired course angle and the inertial speed commands for each follower UAV. The control commands are then converted to the roll angle and the airspeed commands for the autopilot. The theoretical stability proof is rigorously analyzed via the Lyaupunov method. The performance of the proposed control law is compared with the existing vector-field formation guidance scheme via numerical simulation. After the extensive validation using the hardware-in-the-loop simulation environment which includes the mesh network communication system, the flight test are performed to demonstrate not only the performance of the proposed algorithm but also the robustness to the wind disturbance.

INDEX TERMS Multiple fixed-wing UAVs, circular formation, formation guidance, sliding mode control, mesh network, hardware-in-the-loop-simulation, flight test.

I. INTRODUCTION

Recently, with the widespread application of UAVs in various missions, the interest in cooperative operation of multiple UAVs is paid great attention in the civil and military fields. In particular, multiple UAVs performing complex missions simultaneously increase the success rate and efficiency of the mission and also improves situational awareness. As an example of the operation of multiple UAVs, the formation flight is the most basic operational maneuver and is divided into two types of formation, the circular formation and the close formation, in accordance with the formation geometry. Specifically, the circular formation, which refers to a maneuver that circles over target groups while maintaining the constant phase angle between UAVs, is indispensable for searching and surveillance missions of multiple UAVs, which is necessary to increase the monitoring efficiency of the fleet.

To accomplish the formation flight, two technical issues need to be completely addressed: The first one is to design guidance and control law, and the second is to find a way to exchange real-time information among the fleet of UAVs. As for the formation guidance and control, various architectures have been proposed in the literature [1], [2]. One of the architecture is the ''Leader-Follower'' concept, in which the reference commands to enable the formation are calculated upon the status of the leader UAV. In other words, the ''Leader-Follower'' problem is that the follower UAVs consider a leader UAV as a reference point and compute guidance commands to track the point so that the leader-follower keeps the formation for arbitrary maneuvers of the leader UAV [2].

In order to exchange real-time information among the fleet of the UAVs, it is common to use the RF communication network in practice. In this case, each UAV is not only able to broadcast its own navigation data but also to receive the data from other UAVs. Especially for formation flight, the navigation data of each UAV, including measured sensor data and monitoring status, should be shared over the network through a wireless radio channel. In [1], a ground control station (GCS) is responsible for routing data in the network so that it receives the entire navigation data of the UAVs

The associate editor coordinating the review of this manuscript and approving it for publication was Xiwang Dong.

while broadcasting the data throughout the network. Because all data must go through the GCS, there is a disadvantage that the failure of the GCS causes the failure of the entire network. Because of this limitation owing to the centralized communication topology, the decentralized communication topology has been adopted by [3] and the author's previous work [4].

Various algorithms for the formation guidance of multiple UAVs have been studied in the literature. The circular formation guidance algorithm using nonlinear guidance law is proposed in [3]. A waypoint constraint problem on the circular formation is presented in [5] to avoid a mid-air collision among multiple UAVs. The vector-field method and the consensus algorithm are applied for the triangular formation [6]. In [7], the authors present the combination of the circular motion control law and the phase control law to achieve the circular formation. The vector-field guidance technique is the well-studied topic and has the advantage of straightforward implementation [8], [9], [10], [11], [12], [13], [14]. Robust standoff target tracking using the modified vector field guidance [15] ensures globally finite-time stability under unknown wind disturbance. In [16], assuming the standoff tracking problem of multiple UAVs resembles the conical pendulum motion, the authors proposed the design of standoff tracking control by applying the backstepping scheme. Also, the nonlinear model predictive technique [17] and the solution of differential geometry between the UAV and a target [18] are proposed for the standoff target tracking guidance law. In addition, the standoff tracking of a moving target has been studied [19], [20]. The convergent solution of the differential geometry with the bounded speed ratio between the UAV and the target is used to guide the UAV to the standoff geometry [19], while the nonlinear model predictive control is applied to achieve the standoff tracking of moving ground vehicle [21].

Most of aforementioned guidance law only calculates the speed command in order to maintain a fixed phase angle distance between fixed-wing UAVs for the circular formation, while the course angle control is utilized to loiter around the stationary target on ground. However, due to the effect of wind disturbance, the fixed-wing UAV may have difficulties to maintain the circular path and the guidance law needs a control strategy in lateral direction to regulate the radial error. To overcome the wind disturbances and achieve satisfactory standoff tracking, the variable airspeed controller with the adaptive wind estimation scheme [22] is proposed, while the estimated wind is utilized by the Lyapunov-based vector field guidance algorithm [23] and the command filtered backstepping scheme [24].

In this paper, based on the "Leader-Follower" concept, the guidance algorithm for the circular formation flight of multiple fixed-wing UAVs is proposed. In order to regulate the distance error with respect to the moving reference point located at a distance from the leader UAV, the outer loop calculates the desired course angle command and the inertial speed command and the inner loop computes the course rate input to enable the course angle control. The guidance commands are then converted to the roll angle and the airspeed commands for the autopilot. The main contribution is that with a theoretical stability proof of the proposed algorithm the performance is extensively validated via the hardware-in-the-loop simulation as well as the flight test. From this point of view, it can be proven that the proposed algorithm has advantages of the tight performance requirement and the increased system robustness for the formation control of multiple UAVs.

This paper is organized as follows: The basic of the formation geometry is described in Sec. II. The mathematical derivation of the proposed formation control law is presented in Sec. III. A short description of the RF mesh network communication is given in Sec. IV with the communication performance verification. Sec. V discusses the experimental results from the hardware-in-the-loop simulation as well as the flight test, and finally Sec. VI concludes the paper.

II. CIRCULAR FORMATION GEOMETRY

In order to increase surveillance range for ground targets, a fleet of multiple fixed-wing UAVs are assumed to fly at the same altitude while evenly distributed over the circular trajectory around the ground targets. Then, the circular formation guidance problem of the leader-follower UAVs is defined as such that with the leader UAV circling around a fixed-point, the follower UAVs are guided to moving reference points on the circular trajectory. These points move as the leader UAV loiters around the fixed-point while maintaining the relative distances with respect to the leader UAV so as to achieve the circular formation. This section describes how the reference points are calculated only using the navigation data of the leader UAV. In the following derivation, the leader UAV is assumed to move in a counter-clockwise direction, but it is easily modified to consider the case where the leader UAV moves in the opposite direction. The geometric relationship of the circular formation is illustrated in Fig. 1. The angular position of each UAV is referenced by the phase angle defined along the clockwise direction from the inertial North, and the relative angular position of the follower UAV is defined by the difference in phase angle between the leader and the follower UAVs. Assume each UAV turns without sideslip, that is, flying under the coordinated turn condition, the motion of each UAV can be approximately described by the unicycle kinematic equations

$$\begin{aligned} \dot{p}_{\star n} &= V_\star \cos\chi_\star \\ \dot{p}_{\star e} &= V_\star \sin\chi_\star \\ \dot{\chi}_\star &= \omega_\star \end{aligned} \tag{1}$$

where $p_\star = \begin{bmatrix} p_{\star n} & p_{\star e} \end{bmatrix}$ is the inertial position vector, $V_\star$ inertial speed, $\chi_\star$ the course angle, and $\omega_\star$ is the course rate where the subscript $\star = \ell, f, r$ denotes the leader UAV, the follower UAV, and the reference point on the circular trajectory, respectively. The information of the circular trajectory is retrieved from the navigation data of the leader UAV. That

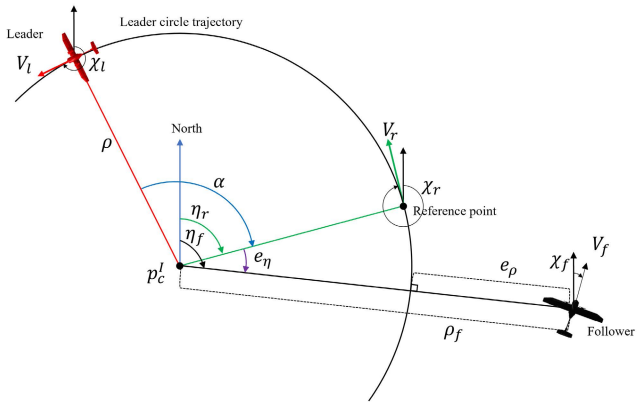

FIGURE 1. Geometric relationship of the circular formation.

is, the center position p_c^I and the radius ρ_r of the circle are calculated from the position vector p_ℓ^I, the course angle χ_ℓ, the roll angle ϕ_ℓ, and the inertial speed V_ℓ of the leader UAV as follows:

$$p_c^I = p_\ell^I + \begin{bmatrix} \rho_r \sin\chi_\ell & -\rho_r \cos\chi_\ell \end{bmatrix}^T = \begin{bmatrix} p_{cn} & p_{ce} \end{bmatrix}^T \quad (2a)$$

$$\rho_r = \left| \frac{V_\ell^2}{g \tan\phi_\ell} \right| \quad (2b)$$

Given the information of the circle, the reference point on the trajectory is calculated as follows:

$$p_r^I = p_c^I + \begin{bmatrix} -\rho_r \sin\chi_r & \rho_r \cos\chi_r \end{bmatrix}^T = \begin{bmatrix} p_{rn} & p_{re} \end{bmatrix}^T \quad (3)$$

where χ_r is calculated by adding the desired phase lag α to the course angle of the leader UAV as $\chi_r = \chi_\ell + \alpha$. The phase angle η_r and the inertial speed V_r of the corresponding reference point are calculated as

$$\eta_r = \tan^{-1}\left(\frac{p_{re} - p_{ce}}{p_{rn} - p_{cn}}\right) \quad (4a)$$

$$V_r = W_n \cos\chi_r + W_e \sin\chi_r + \sqrt{(W_n \cos\chi_r + W_e \sin\chi_r)^2 - (W_n^2 + W_e^2) + V_a^2} \quad (4b)\text{–}(4c)$$

It should be noted that due to the external wind speed the inertial speed needs to adjusted, taking into account the minimum required airspeed command V_a of the fixed-wing UAVs to avoid a stall condition. Subsequently, the reference speed in (4c) has been calculated using the fixed airspeed command in conjunction with the estimated wind velocity using the nonlinear wind disturbance observer [24], [25].

III. FORMATION GUIDANCE LAW

The objective of the proposed guidance law is to make the follower UAV track the reference point on the circular trajectory. The guidance law not only generates a desired course angle command but also a desired inertial speed of the follower UAV in order to regulate the distance errors. Then, the integral sliding mode control scheme is applied to obtain the roll angle command of the fixed-wing UAV to align the course angle to the desired value.

A. PROBLEM FORMULATION

Referring to Fig. 1, it is clear that the distance error can be defined using the polar coordinate system of which the origin is attached at the center of the circle as

$$\begin{aligned} e_\rho &\triangleq \rho_f - \rho_r \\ e_\eta &\triangleq \eta_f - \eta_r \end{aligned} \quad (5)$$

where ρ_f is the radial distance from the center of the circle to the follower UAV and η_f is the angular position of the follower UAV from the North. Note that from Fig. 1 the rate of change of the radial distance and the phase angle of the follower UAV can be derived as,

$$\begin{aligned} \dot{\rho}_f &= V_f \cos(\eta_f - \chi_f) \\ \dot{\eta}_f &= -\frac{V_f}{\rho_f} \sin(\eta_f - \chi_f) \end{aligned} \quad (6)$$

The error system is obtained by differentiating (5) with respect to time using (6) with assumption of $\dot{\rho}_r = 0$ and $\dot{\eta}_r = -\frac{V_r}{\rho_r}$,

$$\dot{e}_\rho = V_f \cos\left(\eta_f - \chi_f\right) \quad (7a)$$

$$\dot{e}_\eta = -\frac{V_f}{\rho_f} \sin\left(\eta_f - \chi_f\right) + \frac{V_r}{\rho_r} \quad (7b)$$

In addition to the distance error states, the error state of the course angle e_χ is defined by the deviation from the desired course, that is, $e_\chi = \chi_f - \chi_d$ where χ_d is the desired course angle command to the follower UAV. Overall, the entire error system is obtained by augmenting the following differential equation,

$$\dot{e}_\chi = \omega_f - \dot{\chi}_d + d_\chi \quad (8)$$

Note that ω_f is the rate of change of the course angle due to the bank-turn maneuver of the follower UAV and d_χ represents the disturbance caused by a non-coordinated turn maneuver under the wind condition. In the normal flight condition under limited bank angle, however, d_χ can be assumed to be upper bounded, or $\sup\{d_\chi\} \le d$.

Note that the error system in (7) and (8) can be regarded as a unicycle system in the polar coordinates. Similar to the unicycle kinematics, this system has two control inputs of the inertial speed V_f and the course rate ω_f. Assuming there exists a feedback control law for the course angle with the input of the course rate, the formation guidance problem turns into a problem of calculating the inertial speed command and the desired course angle command of the follower UAVs. These commands, with the properly tuned low-level autopilot, yield the required control action to guide the follower UAV to the moving reference point along both the longitudinal and the lateral direction to regulate the phase angle error and the radial distance error, respectively.

B. FORMATION GUIDANCE LAW

The proposed formation guidance law aims at reducing the errors in the radial and angular direction of the follower UAV by applying the desired inertial speed V_d and the desired course angle χ_d instead of the control inputs V_f and χ_f of the error system in (7), which is proposed as follows,

$$\mathbf{u}_d = \begin{bmatrix} V_d & \chi_d \end{bmatrix}^T = \begin{bmatrix} \left(k_v e_\eta + \dfrac{V_r}{\rho_r}\right)\rho_f \\ \cos^{-1}\left(\dfrac{-k_\rho e_\rho}{\sqrt{\delta_\rho^2 + e_\rho^2}} + \dfrac{-k_\eta e_\eta}{\sqrt{\delta_\eta^2 + e_\eta^2}}\right) + \eta_f \end{bmatrix} \tag{9}$$

where k_ρ, δ_ρ, k_η, δ_η, and k_v are the positive gain parameters. It should be noted that the guidance parameters k_ρ and k_η in conjunction with δ_ρ and δ_η should be carefully chosen within the range where the argument of the inverse cosine function should conform to the limited domain.

Proposition 1: With the choice of command inputs in (9)*, the radial and the phase angle errors of the error system* (7) *asymptotically tends to zero.*

Proof: Substituting the desired inertial speed V_d and the course angle χ_d for the control inputs V_f and χ_f, one gets the following closed-loop system

$$\begin{aligned} \dot{e}_\rho &= -\rho_f\left(k_v e_\eta + \frac{V_r}{\rho_r}\right)\left(\frac{k_\rho e_\rho}{\sqrt{\delta_\rho^2 + e_\rho^2}} + \frac{k_\eta e_\eta}{\sqrt{\delta_\eta^2 + e_\eta^2}}\right) \\ \dot{e}_\eta &= -\left(k_v e_\eta + \frac{V_r}{\rho_r}\right)\sqrt{1 - \left(\frac{k_\rho e_\rho}{\sqrt{\delta_\rho^2 + e_\rho^2}} + \frac{k_\eta e_\eta}{\sqrt{\delta_\eta^2 + e_\eta^2}}\right)^2} + \frac{V_r}{\rho_r} \end{aligned} \tag{10}$$

where $\cos(\sin^{-1}(\cdot)) = \sqrt{1 - (\cdot)^2} = \sin(\cos^{-1}(\cdot))$ is used for derivation. The equilibrium point of the closed-loop system is first obtained by $\dot{e}_\rho = \dot{e}_\eta = 0$ as

$$\begin{aligned} \dot{e}_\rho = 0 &\iff \frac{k_\rho e_\rho}{\sqrt{\delta_\rho^2 + e_\rho^2}} + \frac{k_\eta e_\eta}{\sqrt{\delta_\eta^2 + e_\eta^2}} = 0 \\ \dot{e}_\eta = 0 &\iff -\left(k_v e_\eta + \frac{V_r}{\rho_r}\right) + \frac{V_r}{\rho_r} = 0 \end{aligned} \tag{11}$$

Subsequently, the equilibrium point of the closed-loop system is simply determined by $e_\rho = e_\eta = 0$. In order to show the stability of the equilibrium point, first note that the right hand sides of (10) are continuously differentiable functions in a neighborhood of the equilibrium point under the assumption $\rho_r > 0$. It follows that one can linearize the error system at the equilibrium point, to obtain the following approximated linear system:

$$\begin{bmatrix} \dot{e}_\rho \\ \dot{e}_\eta \end{bmatrix} \approx \begin{bmatrix} -\rho_r\left(k_v + \dfrac{V_r}{\rho_r}\right) & -V_r\dfrac{k_\eta}{\delta_\eta} \\ 0 & -k_v \end{bmatrix} \begin{bmatrix} e_\rho \\ e_\eta \end{bmatrix} \tag{12}$$

It is straightforward to check that the eigenvalues of the Jacobian matrix are all strictly negative, as the parameters k_v, V_r, and ρ_r are assumed to be positive. By Theorem 4.7 in [26], the origin is an asymptotically stable equilibrium point, then the radius error e_ρ and the angular error e_η of the closed-loop system (10) asymptotically tends to zero. □

Remark 1: In addition to the existence of the Jacobian matrix, the Jacobian matrix in (12) is bounded and Lipschitz continuous on the neighborhood of the origin. Therefore, with the Jacobian matrix being Hurwitz the origin is determined as an exponentially stable equilibrium point for the closed-loop system (10). Furthermore, according to the converse Lyapunov theorem there exists a positive definite Lyapunov function $V_1(e_\rho, e_\eta)$ which satisfies the inequalities

$$\begin{aligned} c_1||\mathbf{x}||^2 \le V_1(\mathbf{x}) \le c_2||\mathbf{x}||^2 \\ \dot{V}_1 \le -c_3||\mathbf{x}||^2 \end{aligned} \tag{13}$$

where $\mathbf{x} = \begin{bmatrix} e_\rho & e_\eta \end{bmatrix}^T$ and for some positive constants c_1, c_2, and c_3 [26].

C. COURSE ANGLE TRACKING

This section describes the course angle tracking control to make the follower UAV track the desired course angle via bank-turn maneuver. The course tracking controller supplements the formation guidance law by quickly regulating the course error e_χ so that the actual course angle follows the desired value in (9). As a result, the assumption of the command input for the formation guidance law is satisfied. In addition, the controller calculates a course rate command ω_f designed via the integral sliding mode control scheme, which can effectively handle the bounded disturbance. The course rate command is converted to a roll command, which is then fed into the low-level autopilot.

A variable for sliding surface is defined as

$$s \triangleq e_\chi + k_\omega \int e_\chi dt \tag{14}$$

where k_ω is an integral control gain that determines the motion of e_χ on the sliding surface $s = 0$. Taking into account the model of the error heading angle in (8), suppose that there exists a control action which makes the sliding surface invariant, or $s \equiv 0$. Then, the trajectory of e_χ on the sliding surface is simply described by

$$\dot{e}_\chi = -k_\omega e_\chi \tag{15}$$

which dictates that e_χ converges exponentially to the origin with the value of the time constant k_ω.

Now, in order to design a control law which drives the state e_χ to a point on the sliding surface from outside, one considers a Lyapunov candidate function, $V_2(s) = (1/2)s^2$, the time derivative of the function is obtained by utilizing the kinematic model (8)

$$\dot{V}_2 = s(\omega_f - \dot{\chi}_d + d_\chi + k_\omega e_\chi) \tag{16}$$

Recall that the wind disturbance d_χ is assumed to be upper bounded, after rearranging the right hand side of (16), one can get the following,

$$\dot{V}_2 \le |s|\left\{|k_\omega e_\chi - \dot{\chi}_d| + d\right\} + s\omega_f \tag{17}$$

The proposed course rate control law is given as follows,

$$\omega_f = -\Big\{|k_\omega e_\chi - \dot{\chi}_d| + d + \omega_0\Big\}\text{sign}(s) \tag{18}$$

where sign(·) is the signum function and ω_0 is a positive parameter to render inside the bracket strictly positive.

Proposition 2: Given the system of the course error in (8)*, the course rate control* ω_f *in* (18) *makes the course error of the closed-loop system towards zero in finite time.*

Proof: By substituting the control (18) into (16), one gets

$$\dot{V}_2 \le -\omega_0|s| \tag{19}$$

If one defines a function $W = \sqrt{V_2} = |s|$, then the right hand derivative of the function is computed as follows,

$$D^+W = \frac{d}{dt}\sqrt{V_2} = \frac{\dot{V}_2}{2\sqrt{V_2}} \le \frac{-\omega_0|s|}{2|s|} = -\frac{\omega_0}{2} \tag{20}$$

By integrating both sides, one gets the solution as

$$|s(t)| \le |s(t=0)| - \frac{1}{2}\omega_0 t \tag{21}$$

By the comparison lemma and with the assumption of W lower bounded by zero, the trajectory of $|s(t)|$ will approach to the solution of $|s(\infty)| = 0$, that is, the sliding variable s will enter the sliding surface $s = 0$ in finite time and stays on the surface afterwards. Subsequently, by (15) the error state e_χ on the sliding surface goes to zero exponentially. □

Remark 2: For actual implementation of the proposed controller in (18), one needs to compute $\dot{\chi}_d$, which is derived analytically as

$$\begin{aligned}\dot{\chi}_d &= \frac{d}{dt}\left\{\cos^{-1}\left(\frac{-k_\rho e_\rho}{\sqrt{\delta_\rho^2 + e_\rho^2}} + \frac{-k_\eta e_\eta}{\sqrt{\delta_\eta^2 + e_\eta^2}}\right)\right\} + \dot{\eta}_f \\ &= \frac{-1}{\sqrt{1-X^2}}\left[\frac{-k_\rho \delta_\rho^2 \dot{e}_\rho}{(\delta_\rho^2 + e_\rho^2)^{\frac{3}{2}}} + \frac{-k_\eta \delta_\eta^2 \dot{e}_\eta}{(\delta_\eta^2 + e_\eta^2)^{\frac{3}{2}}}\right] + \dot{\eta}_f \end{aligned} \tag{22}$$

where the symbol X denotes the argument of the arc cosine function, $\dot{e}_\rho$, $\dot{e}_\eta$, and $\dot{\eta}_f$ are calculated using (7a), (7b), and (6), respectively. However, due to the complexity of the analytical derivative, the derivative of the desired course rate can be calculated by applying a first-order differentiation filter to the desired course angle command. The transfer function is chosen in the form of $s/(\tau s + 1)$ with a time constant τ tuned carefully [27].

As mentioned earlier, the desired course rate is realized via bank-turn maneuver assuming the coordinated turn condition. Accordingly, a roll angle command to the autopilot is computed as follows [28],

$$\phi_c = \tan^{-1}\frac{\omega_f V_f}{g\cos(\chi_f - \psi_f)} \tag{23}$$

where ψ_f is the heading angle of the follower UAV.

D. OVERALL STABILITY ANALYSIS

The circular formation of leader-follower UAVs is accomplished by regulating the phase angle error and the radial distance error of the follower UAV with respect to the moving reference point determined by (4). For this, the formation guidance law consists of two main control loops: The outer loop and the inner loop. The outer loop calculates the inertial speed command as well as the course angle command to regulate the distance error, while the inner loop enables following the course angle command with the course rate control. In this section, the overall stability of the entire control loops is presented.

Theorem 1: Consider the error kinematic system described in (7) and (8). Given the desired speed and the course angle command in (9), and the course rate control ω_f in (18), the error states e_ρ, e_η, and e_χ converge to zero simultaneously.

Proof: Provided the sliding variable s remains zero, the error state e_χ spontaneously converges to zero as shown in (15). Subsequently, with a slight abuse of notation, the stability of error state e_χ is replaced with the stability of the sliding variable s, which implies that the error states e_ρ and e_η as well as the sliding variable s should be attracted to zero near the origin. To this end, one defines a Lyapunov candidate function, $V(\mathbf{z}) = V_1(\mathbf{x}) + V_2(s)$ where $\mathbf{z}$ denotes the augmented state as $\mathbf{z} = [\mathbf{x} \;\; s]^T$. By the definition of the Lyapunov function V_1 and V_2, V is positive definite and decrescent with two class-$\mathcal{K}$ functions as

$$\min\{c_1, 0.5\}\,\|\mathbf{z}\|^2 \le V(\mathbf{z}) \le \max\{c_2, 0.5\}\,\|\mathbf{z}\|^2 \tag{24}$$

Differentiate with respect to time, and then one applies the desired commands $\mathbf{u}_d$ in (9) and the course rate control ω_f in (18) to get

$$\begin{aligned}\dot{V} &= \dot{V}_1 + \dot{V}_2 \\ &\le -c_3\,\|\mathbf{x}\|^2 - \omega_0|s| \end{aligned} \tag{25}$$

Suppose s is sufficiently small, or, $|s| < 1$, it follows

$$\begin{aligned}\dot{V} &\le -c_3\,\|\mathbf{x}\|^2 - \omega_0 s^2 \\ &\le -\min\{c_3, \omega_0\}\,\|\mathbf{z}\|^2 \end{aligned} \tag{26}$$

It is immediate from (26) that $\dot{V}$ is negative definite, or $\dot{V}$ is upper bounded by a class-$\mathcal{K}$ function with negative sign. Therefore, by the Lyapunov theorem the augmented state $\mathbf{z}$ exponentially tends to zero. In other words, the error states e_ρ and e_η approaches zero in finite time, so does the sliding variable s. After s sufficiently close to zero, the motion on the sliding surface described in (15) makes the course angle error e_χ tend to zero. □

E. NUMERICAL SIMULATION

In order to validate the performance of the proposed guidance law, a comparative study was conducted through numerical simulations. In this study, the proposed control law is compared with the standoff distance and phase angle control schemes using the vector field [10] and the relative phase

angle guidance [3]. A simple 3-dof kinematic model was utilized to simulate the trajectory of the leader and the follower UAVs.

$$\dot{p}_n = V_a \cos\psi + W_n \tag{27a}$$
$$\dot{p}_e = V_a \sin\psi + W_e \tag{27b}$$
$$\dot{\psi} = \frac{g}{V_a}\tan\phi \tag{27c}$$

where p_n and p_e are the vehicle's position with respect to NED frame, and V_a is the airspeed, ψ is the heading angle, and ϕ is the roll angle. In addition, in order to closely approximate actual response to the guidance commands, the airspeed-hold and roll-hold autopilot loops are assumed to be first-order systems [28]

$$\dot{\phi} = \omega_\phi(\phi^c - \phi) + d_\phi \tag{28a}$$
$$\dot{V}_a = \omega_V(V_a^c - V_a) + d_V \tag{28b}$$

where ϕ_c and V_a^c are the roll angle command and airspeed command, while ω_ϕ and ω_V correspond to the natural frequency of each control loop. It should be noted that the disturbance terms d_ϕ and d_V are deliberately included in the autopilot model to evaluate the robustness of the proposed algorithm. These terms are supposed to be induced by external wind, which might result in the steady state error of both control loops. Since the formation guidance law should compensate the command errors due to such disturbances, it is important to test the robustness in the simulation environment before the actual flight test.

The comparative simulation results between the proposed algorithm and the existing algorithms are shown in Fig. 2. For a fair comparison, the same wind speed was assumed and estimated through the wind disturbance observer. It should be noted that with a slight modification the existing algorithms was made to utilize the estimated wind speed explicitly. On the other hand, it is assumed that small disturbance due to the asymmetric roll maneuver remains in the simulation. The error states e_ρ, e_η, and e_χ are plotted compared in Fig. 2(a), 2(b), and 2(c), respectively. The solid line represents the history of the error states using the proposed guidance law, the dashed line indicates the error states from the vector-field method, and the dotted line for the relative phase angle guidance control. As shown in the figures, it appears that both the vector-field method and the relative phase angle guidance have a certain steady-state error. Despite the explicit compensation using the estimated wind speed, this error can be attributed to an indirect effect of the asymmetric roll disturbance in (28). Thus, without any proper control action against the disturbance, these methods become ineffective in reducing the steady error. In contrast, the proposed guidance law is effective in eliminating the wind disturbance because the reference trajectory is calculated using the navigation data of the leader UAV in conjunction with the estimated wind speed information, as shown in Fig. 2.

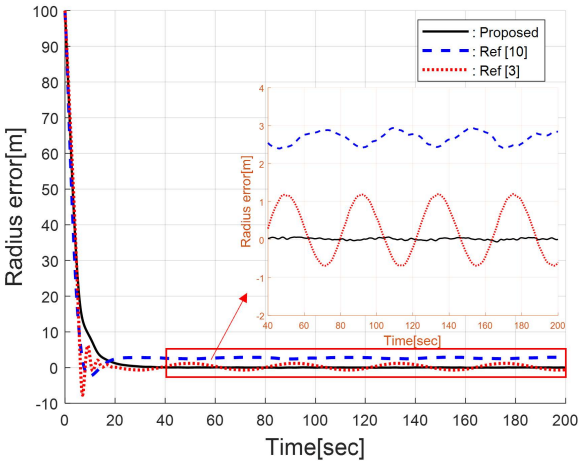

(a) History of radial error e_ρ

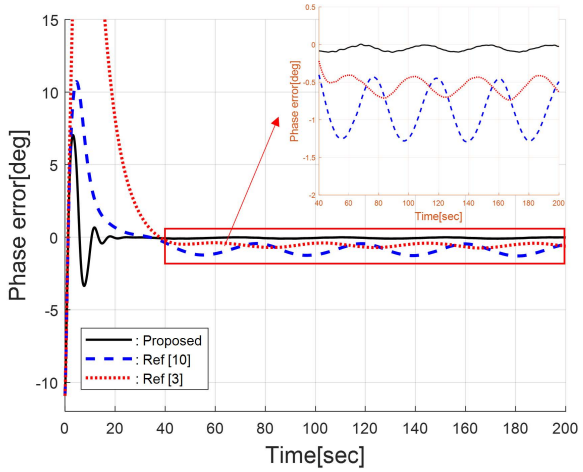

(b) History of phase angle error e_η

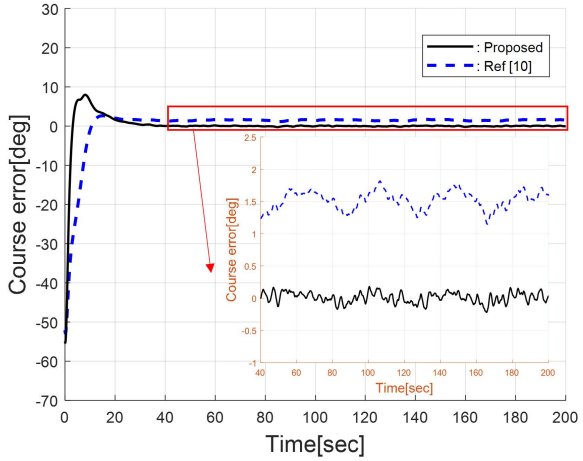

(c) History of course angle error e_χ

FIGURE 2. Simulation results for comparative study of circular formation guidance.

IV. EXCHANGING NAVIGATION DATA VIA MESH NETWORK

In order to implement the proposed guidance law, the follower UAVs need to obtain the navigation information of the leader UAV. For this purpose, multiple RF wireless modems

are opted to exchange the information between UAVs and the ground station over the mesh network, as shown in Fig. 3. Unlike centralized communication topology, the mesh network is regarded decentralized communication topology, hence it allows all data generated by an arbitrary node to arrive at the nodes over the network without a need of router node. This scheme can avoid the failure of the entire network due to a single failure of the router node. In general, within mesh network, each node is able to not only broadcast its own information, but also receive the information of others. In addition, in order to ensure the robust data transmission between arbitrary source and destination nodes, a network packet needs to be created and sent including the source address [3], [4].

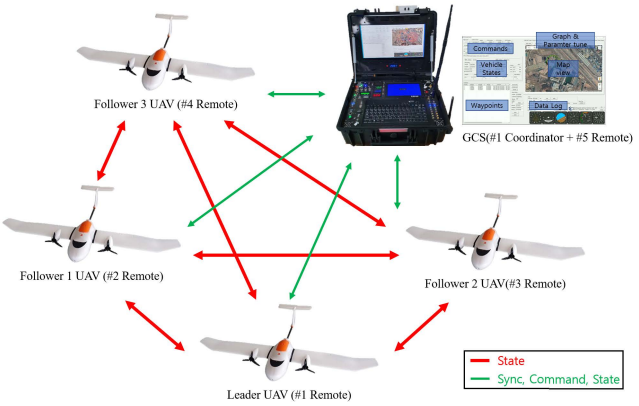

FIGURE 3. Configuration of the mesh network.

A. MESH NETWORK CONFIGURATION

In this study, a set of six 900MHz RF modems by the Microhard Corp. (one for coordinator and five for remote nodes) are incorporated to establish the network for data sharing. The configuration of mesh-network is illustrated in Fig. 3. In this configuration, the coordinator has a role of monitoring the network and synchronizing each modem in the network. Four UAVs and one ground control station (GCS) are utilized as the remote nodes of the network. By adding the GCS in the network, the ground operator can also monitor the status of each UAV while sending appropriate commands to them. A custom mavlink packet is used to share the information including the UAV's navigation data and other essential data for multi-UAVs operation, which includes the GPS time, GPS position fix, the attitude angles, the velocity of the vehicle, to name a few. On the other hand, for the sake of short transmission time, the UAV data packet is composed of binary data, which has the size of 61 bytes and is sent at the rate of 5 Hz. The data throughput rate of each UAV is about 2.44 [kbps] and the overall throughput rate of five remotes is about 12.2 [kbps], which is much lower than the maximum link rate of 276 kbps of the RF modem.

In the mesh configuration, because the remote nodes need to frequently transmit its own information, each remote is necessary to choose an appropriate channel among the available network channels. By doing this, it is possible to prevent data collision while maximizing the communication throughput. The carrier sense multiple access (CSMA), or so called ALOHA channel access mode, is adopted by the RF modem. After determining availability of the channel by measuring the level of the radio signal and comparing with the carrier sense threshold, the modem can initiate the transmission. However, if the channel is unavailable, the modem will select another random ALOHA slot to begin its data transmission. In this research, the carrier sense threshold is set to -50 [dBm] taking into account the RF environment nearby the flight field. In addition, for the sake of the robustness of data communication, the packet should be retransmitted in a noisy environments or when weak signal received. This is done by re-sending the same packet unless acknowledged by the recipient in order to ensure data reaches its intended destination. By increasing the number of retransmission attempts the communication robustness is enhanced, however, at the cost of overall throughput reduction. Subsequently, the remote node of the GCS should be set higher than the remote node of the UAVs because it transmits command data aperiodically to each UAV.

B. PERFORMANCE EVALUATION VIA GROUND TEST

The ground test is conducted to verify the communication performance of the mesh network. To this end, the mesh network emulator developed in-house is utilized to simulate the network system. The emulator system consists of the RF modem hardware and the custom PC software to send/receive the packet while recording the data for further analysis. The architecture of the ground test is depicted in Fig. 4.

The size of the test packet is chosen to be same as the UAV data packet. Instead of navigation data, however, the test packet contains the precise transmission time and reception time to evaluate the packet latency and the incremental index data to check whether there are missing packets. This incremental index is used to assess the communication success rate. During the test, the node #0 corresponds to the ground station and only receives packets from other nodes without transmitting any data. On the other hand, the nodes #1 to #4, which has the role of the UAV node, not only send the test packets at the rate of 5 Hz but also receive the packet originated from other nodes.

In order to simulate the communication environment in the flight test, first notice that the UAVs fly at the altitude of 100 meters and the separation distance between UAVs is about 50 meters for the formation flight. Under this situation, the power loss of the RF signal will occur due to the spatial distance between nodes. Subsequently, to reflect the flight environment as closely as possible through the ground setup, the antenna of each modem are placed 1 meter apart, and 20dB attenuators are inserted on the transmission line to the antenna. This attenuator permits weakening the RF signal corresponding to the path loss of about 100 meters, so that the reliability of the ground test can be justified. Table 1

summarizes the ground test results. Since the average success rate is about 97% and the packet latency is less than approximately 30 msec, it has been confirmed that the mesh network has sufficient communication performance for a group of four UAVs to exchange data in almost real time.

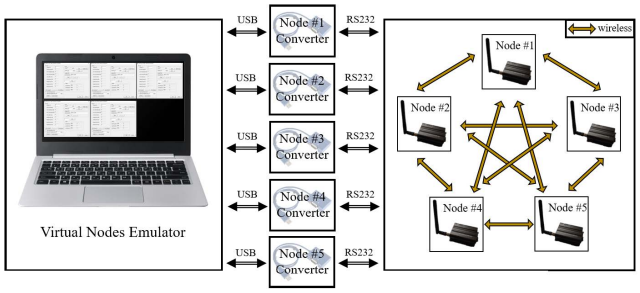

FIGURE 4. Mesh network ground test.

FIGURE 5. Test-bed platform of four fixed-wing UAVs.

TABLE 1. Results of ground communication test.

Node	Sent Packet	Received packet		Success rate(%)	Latency (ms)
#0	0	#1	3164	98.54	23.1
		#2	3178	98.96	23.1
		#3	3138	97.72	25.1
		#4	3093	96.32	24.8
#1	3211	#2	3178	98.96	24.5
		#3	3134	97.61	26.8
		#4	3089	96.21	27.0
#2	3211	#1	3171	98.75	24.8
		#3	3141	97.82	26.9
		#4	3089	96.21	26.9
#3	3211	#1	3171	98.75	23.8
		#2	3178	98.96	23.4
		#4	3089	96.21	25.4
#4	3211	#1	3171	98.75	24.5
		#2	3178	98.96	23.5
		#3	3138	97.72	25.7

V. EXPERIMENTAL VALIDATION

The performance of the proposed circular formation guidance law is first evaluated through a hardware-in-the-loop simulation (HILS) environment and then validated via the flight tests

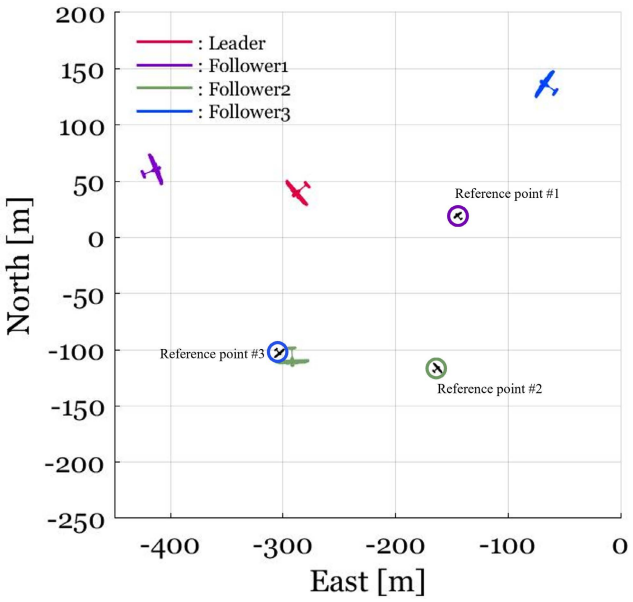

(a) Initial formation geometry of four UAVs

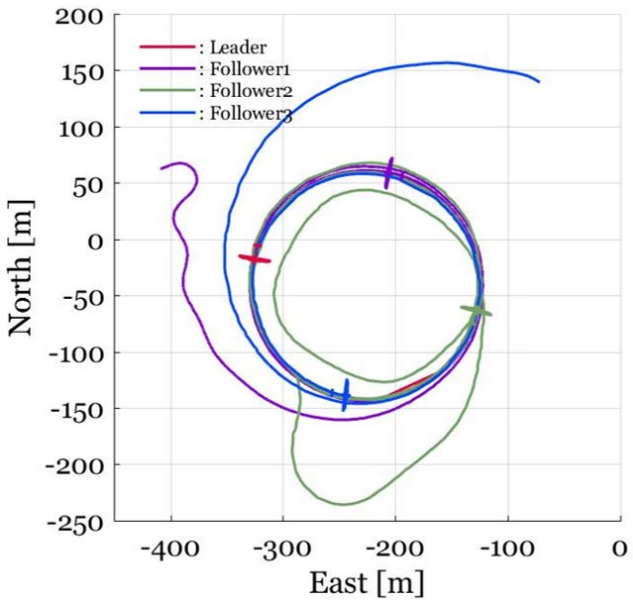

(b) 2-dimensional trajectory of UAVs

FIGURE 6. Hardware-in-the-loop simulation results for circular formation.

using the test-bed platforms. Each test-bed platform includes a fixed-wing UAV and the avionics system which consists of an in-house flight control computer, a GPS receiver, a suite of inertial sensors, a RF modem, an airspeed sensor, and so on. The fixed-wing UAVs are shown in Fig. 5 of which the specifications are summarized in Tab. 2 [4].

A. PERFORMANCE VALIDATION VIA HILS

The hardware-in-the-loop simulation (HILS) environment makes it possible to verify the seamless integration of both the hardware and software by imposing the same flight condition. In particular, the user interface which includes command uploading and status monitoring via the actual communication hardware is extensively verified for various

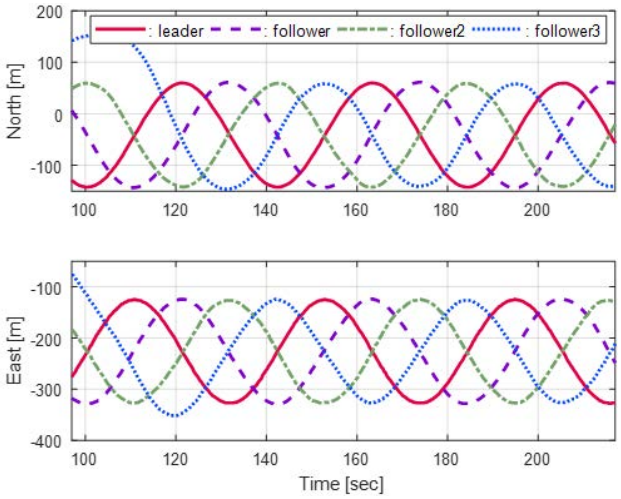

FIGURE 7. Position histories of UAVs.

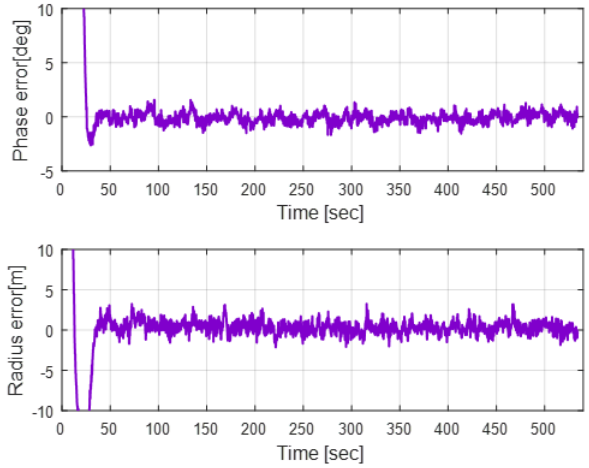

(a) Error states: phase angle, radius

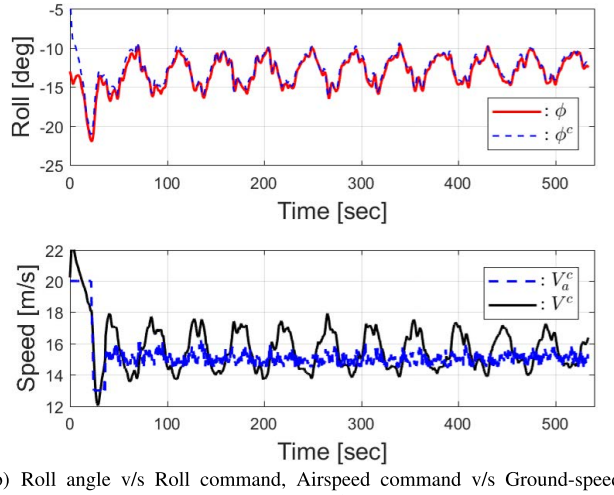

(b) Roll angle v/s Roll command, Airspeed command v/s Ground-speed command

FIGURE 8. Flight test result of follower1 UAV. (a) Upper plot shows the phase angle error and lower plot shows the radius error. (b) Upper plot compares the roll and the roll command in dashed line, while the lower plot shows the airspeed command compared with the ground-speed command.

scenarios. The detailed description of the HILS environment can be found in [29].

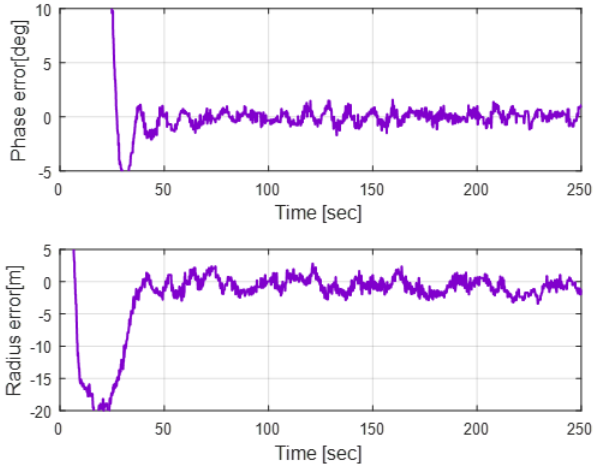

(a) Error states: phase angle, radius

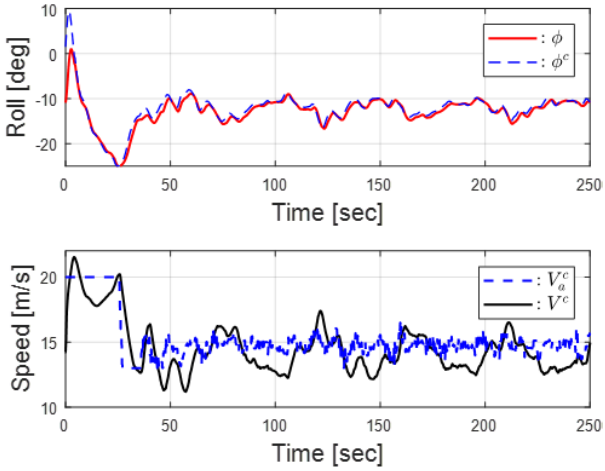

(b) Roll angle v/s Roll command, Airspeed command v/s Ground-speed command

FIGURE 9. Flight test results of folower2 UAV. (a) Upper plot shows the phase angle error and lower plot shows the radius error. (b) Upper plot compares the roll and the roll command in dashed line, while the lower plot shows the airspeed command compared with the ground-speed command.

TABLE 2. Test-bed specification.

	Skywalker eve-2000
Wingspan/Length	2240/1270 mm
Total weight	4.6kg(including battery)
Cruise speed	15 – 22 m/s
Propulsion System	Twin-prop BLDC motor
Battery	6s 10000 mAh
Flight Control System	Cupido FCC (in-house)

During the simulation, the leader UAV flies at the desired altitude of 100 meters AGL and the desired airspeed of 15 m/s. Also, the leader UAV is commanded to loiter around the circular path with a radius of 100 meters under no wind condition. It follows that at the command of the ground operator, three follower UAVs initiate the circular formation to keep the 90 degrees of phase angle difference between the UAVs on the circular trajectory. Taking into account the maximum turn rate and the stall speed of the test-bed airframe, the follower UAVs have the command limits of 12 – 20 m/s and

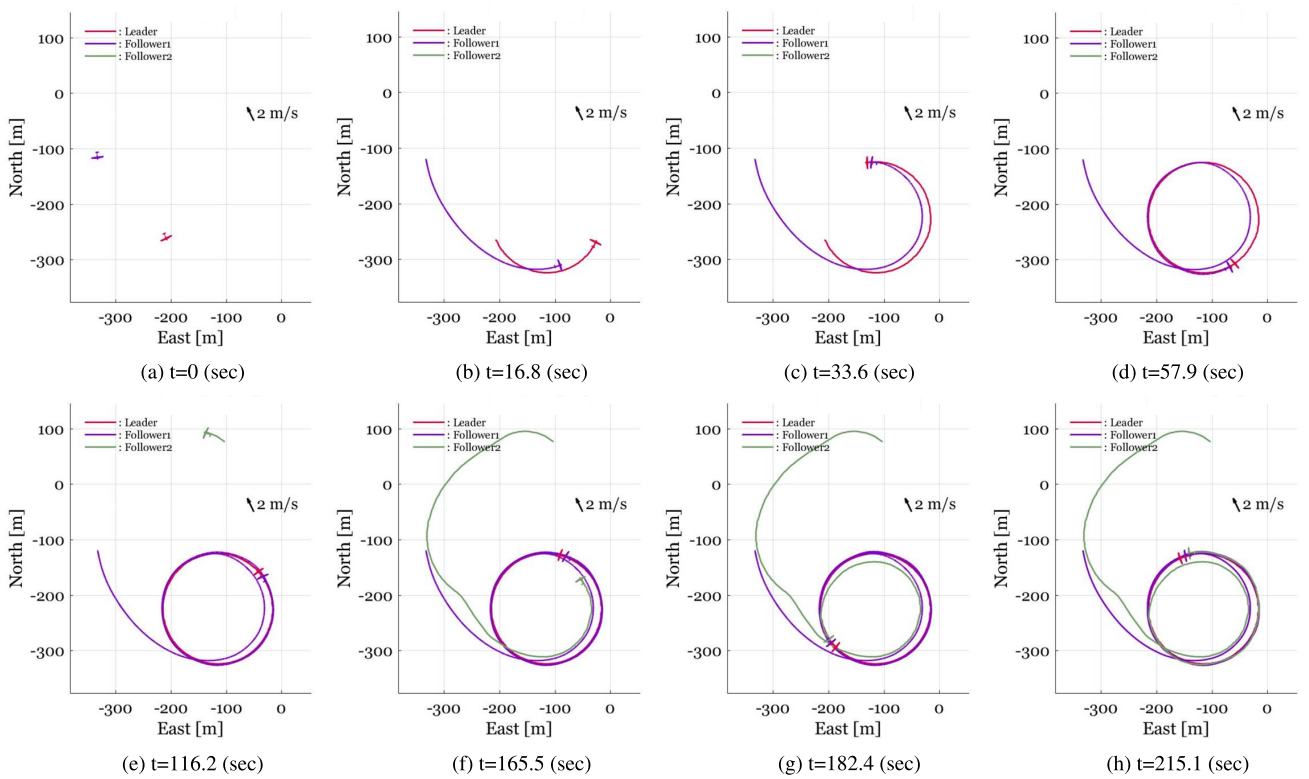

FIGURE 10. Flight test results for selected 2-dimensional trajectory of three fixed-wing UAVs.

-45 - 45 deg in the airspeed and the roll angle, respectively. The gain parameters used in the simulation are listed in Tab. 3.

TABLE 3. The design parameters for the HILS.

k_ρ/δ_ρ	k_η/δ_η	k_ω	ω_0	d	k_v
0.75/80	0.25/35	0.1	0.05	0.1	0.2

In order to figure out the control characteristics for various initial conditions, a test scenario was created such that three follower UAVs have different initial locations and headings when commencing the formation guidance. Figure 6(a) depicts the situation when the initial formation geometry of four UAVs where three reference points for the follower UAVs are marked by the small aircraft circle symbols. The initial conditions of each follower UAV are specified as follows,

$$\text{follower\#1} : \left[p_{n0}\ p_{e0}\right]^T = \left[-409\ 62\right]^T \text{m}, \quad \psi_0 = 67^\circ$$
$$\text{follower\#2} : \left[p_{n0}\ p_{e0}\right]^T = \left[-115\ -292\right]^T \text{m}, \ \psi_0 = 178^\circ$$
$$\text{follower\#3} : \left[p_{n0}\ p_{e0}\right]^T = \left[-145\ 156\right]^T \text{m}, \quad \psi_0 = -85^\circ$$

The hardware-in-the-loop simulation results are illustrated in Fig. 6(b). The red, purple, green, and blue lines indicate the flight trajectories of the leader, follower#1, follower#2, and follower#3, respectively. It is shown that the follower#1 performs a sharp turn during the initial transient to catch up the approaching reference point, while the follower#2 slowly catches up the corresponding reference point after one more round of circular trajectory. Once each UAV has caught up the corresponding reference point, it maintains the circular formation by keeping the distance error from the reference point to a minimum. Figure 7 displays the time history of the inertial position of the UAVs from 95 seconds after the start command of the formation, which further shows that there exists 90 degree phase difference between UAVs in the steady state.

B. PERFORMANCE VALIDATION VIA FLIGHT TEST

After confirming the seamless integration of the proposed algorithm through the HILS system, a flight test is conducted using a fleet of three UAVs. While the leader UAV loiters with a radius of 100 meters around a predefined point at the constant airspeed 15 m/s, two follower UAVs are sequentially commanded to initiate the circular formation according to the ground control.

The target geometry of the formation flight is that the follower#1 and the follower#2 maintain the phase angle difference of 5 and 10 degrees with the leader UAV, respectively. The test was conducted under the calm wind speed of approximate 2 m/s, in order to minimize the adverse effect of the wind disturbance on the formation geometry. In addition, the follower UAVs are vertically separated from the leader UAV at a distance of 5 and 10 meters, respectively, to prevent possible mid-air collision. The design parameters for the

FIGURE 11. Circular formation flight test of three fixed-wing UAVs.

flight test has been adjusted based on the values used in the HILS test. The tuned parameters are listed in Tab. 4.

TABLE 4. The design parameters for the flight test.

k_ρ/δ_ρ	k_η/δ_η	k_ω	ω_0	d	k_v
0.75/70	0.25/30	0.08	0.05	0.15	0.3

The flight test results for several time steps are shown in Fig. 10. At the start of the formation control the follower#1 flies behind the leader UAV(a) and then begins to chase the leader UAV along the circular path(b). After going through the initial transient, the follower#1 tracks the moving reference point of 5 degrees behind the leader and continues to fly along the circular path ((c) and (d)).

Figure 10(e) shows the follower#2 joins the formation control from the intermediate loitering orbit. After that, the follower#2 goes through the initial transient to quickly track the reference point (f), which ends up with the circular formation of three UAVs ((g) and (h)).

The tracking errors as well as the guidance commands for each follower UAV are shown in Fig. 8 and Fig. 9. The error states of the radius and the phase angle are depicted in Fig. 8(a) and Fig. 9(a). From the plots, it can be seen that the phase angle error is tightly bounded by ± 1.5 degrees while the radial error by ± 2 meters, which proves that the tracking performance of the proposed algorithm satisfies the high precision requirement for formation flight.

The guidance commands for the follower#1 are illustrated in Fig. 8(b). In the first plot the dashed line denotes the roll angle command from the guidance law while the solid line shows the roll angle state. The periodic oscillation of the roll command is closely related to the direction of the external wind around the circular path, because the fixed-wing UAV needs to adjust its bank angle to maintain the course dependent on the crosswind direction. On the other hand, in the second plot, the ground speed command marked with solid line is also periodically adjusted in order to maintain the nominal airspeed of 15 m/sec regardless of the total speed variation along the circular path. Figure 9(b) shows the guidance commands for the follower#2 in detail. Overall, the proposed algorithm generates appropriate guidance commands for stable formation performance under wind condition. Finally, the left picture of Fig. 11 shows a photo taken with a ground camera during a flight test, while the right picture shows an aerial view of the formation flight taken from an onboard camera of the fourth UAVs flying nearby.

VI. CONCLUSION

The circular formation guidance control law for multiple fixed-wing UAVs is presented. Based on the formation geometry calculated only using the navigation data of the leader UAV, the proposed guidance law computes the desired course angle and the inertial speed command as the outer loop commands to guide each follower UAV to the moving reference

point. As the inner loop control, the integral sliding mode control for the course angle makes it possible to eliminate the steady-state error caused by the wind disturbance, enabling tight heading control performance. The control commands are then converted to the roll angle and the airspeed commands for the autopilot. The theoretical proof is provided to prove the stability of the proposed algorithm. The performance of the proposed control law is validated via the hardware-in-the-loop simulation environment which includes the mesh network communication system, and then the flight demonstration is conducted. The proposed algorithm has advantages of the tight performance requirement and the robustness to the wind disturbance to achieve the formation control of multiple UAVs.

REFERENCES

[1] D. I. You and D. H. Shim, "Autonomous formation flight test of multi-micro aerial vehicles," *J. Intell. Robotic Syst.*, vol. 61, nos. 1–4, pp. 321–337, Jan. 2011, doi: 10.1007/s10846-010-9481-0.
[2] Q. Zhang, "Modeling, analysis, and control of close formation flight," Ph.D. dissertation, Dept. Aerosp. Sci. Eng., Univ. Tolonto, Toronto, ON, USA, 2019. [Online]. Available: http://hdl.handle.net/1807/94080
[3] C. Park, N. Cho, K. Lee, and Y. Kim, "Formation flight of multiple UAVs via onboard sensor information sharing," *Sensors*, vol. 15, no. 7, pp. 17397–17419, Jul. 2015. [Online]. Available: https://www.mdpi.com/1424-8220/15/7/17397
[4] S. Kim, H. Cho, and D. Jung, "Evaluation of cooperative guidance for formation flight of fixed-wing UAVs using mesh network," in *Proc. Int. Conf. Unmanned Aircr. Syst. (ICUAS)*, Sep. 2020, pp. 289–294.
[5] M. Kim and Y. Kim, "Multiple UAVs nonlinear guidance laws for stationary target observation with waypoint incidence angle constraint," *Int. J. Aeronaut. Space Sci.*, vol. 14, no. 1, pp. 67–74, Mar. 2013.
[6] H. G. De Marina, Z. Sun, M. Bronz, and G. Hattenberger, "Circular formation control of fixed-wing UAVs with constant speeds," in *Proc. IEEE/RSJ Int. Conf. Intell. Robots Syst. (IROS)*, Sep. 2017, pp. 5298–5303.
[7] L. Jin, S. Yu, and D. Ren, "Circular formation control of multiagent systems with any preset phase arrangement," *J. Control Sci. Eng.*, vol. 2018, Feb. 2018, Art. no. 9162358, doi: 10.1155/2018/9162358.
[8] H. Oh, S. Kim, H.-S. Shin, and A. Tsourdos, "Coordinated standoff tracking of moving target groups using multiple UAVs," *IEEE Trans. Aerosp. Electron. Syst.*, vol. 51, no. 2, pp. 1501–1514, Apr. 2015.
[9] E. W. Frew, D. A. Lawrence, and S. Morris, "Coordinated standoff tracking of moving targets using Lyapunov guidance vector fields," *J. Guid., Control, Dyn.*, vol. 31, no. 2, pp. 290–306, Mar. 2008, doi: 10.2514/1.30507.
[10] S. Yoon and Y. Kim, "Decentralized phase angle control for standoff tracking using multiple unmanned aircraft," in *Proc. ICCAS*, Oct. 2010, pp. 2124–2127.
[11] J. Zhang, J. Yan, P. Zhang, and X. Kong, "Design and information architectures for an unmanned aerial vehicle cooperative formation tracking controller," *IEEE Access*, vol. 6, pp. 45821–45833, 2018.
[12] S. Lim, Y. Kim, D. Lee, and H. Bang, "Standoff target tracking using a vector field for multiple unmanned aircrafts," *J. Intell. Robot. Syst.*, vol. 69, nos. 1–4, pp. 347–360, Jan. 2013, doi: 10.1007/s10846-012-9765-7.
[13] D. Kingston and R. Beard, "UAV splay state configuration for moving targets in wind," in *Advances in Cooperative Control and Optimization*. Berlin, Germany: Springer, 2007, pp. 109–128.
[14] T. Z. Muslimov and R. A. Munasypov, "Consensus-based cooperative circular formation control strategy for multi-UAV system," in *Proc. Int. Russian Autom. Conf. (RusAutoCon)*, Sep. 2019, pp. 1–8.
[15] N.-M.-T. Kokolakis and N. T. Koussoulas, "Robust standoff target tracking with finite-time phase separation under unknown wind," *J. Guid., Control, Dyn.*, vol. 44, no. 6, pp. 1183–1198, Jun. 2021.
[16] S. Yoon, S. Park, and Y. Kim, "Circular motion guidance law for coordinated standoff tracking of a moving target," *IEEE Trans. Aerosp. Electron. Syst.*, vol. 49, no. 4, pp. 2440–2462, Oct. 2013.
[17] S. Kim, H. Oh, and A. Tsourdos, "Nonlinear model predictive coordinated standoff tracking of a moving ground vehicle," *J. Guid., Control, Dyn.*, vol. 36, no. 2, pp. 557–566, Mar. 2013, doi: 10.2514/1.56254.
[18] H. Oh, S. Kim, H.-S. Shin, B. A. White, A. Tsourdos, and C. A. Rabbath, "Rendezvous and standoff target tracking guidance using differential geometry," *J. Intell. Robotic Syst.*, vol. 69, nos. 1–4, pp. 389–405, Jan. 2013, doi: 10.1007/s10846-012-9751-0.
[19] Z.-Q. Song, H.-X. Li, C.-L. Chen, X.-Z. Zhou, and F. Xu, "Coordinated standoff tracking of moving targets using differential geometry," *J. Zhejiang Univ. Sci. C*, vol. 15, no. 4, pp. 284–292, Apr. 2014.
[20] H. Oh, S. Kim, A. Tsourdos, and B. A. White, "Decentralised standoff tracking of moving targets using adaptive sliding mode control for UAVs," *J. Intell. Robotic Syst.*, vol. 76, no. 1, pp. 169–183, Sep. 2014, doi: 10.1007/s10846-013-9864-0.
[21] H. Oh, S. Kim, A. Tsourdos, and B. White, "Road-map assisted standoff tracking of moving ground vehicle using nonlinear model predictive control," in *Proc. Amer. Control Conf. (ACC)*, Jun. 2012, pp. 4263–4268.
[22] T. H. Summers, M. R. Akella, and M. J. Mears, "Coordinated standoff tracking of moving targets: Control laws and information architectures," *J. Guid., Control, Dyn.*, vol. 32, no. 1, pp. 56–69, Jan. 2009.
[23] S. Zhu, D. Wang, and Q. Chen, "Standoff tracking control of moving target in unknown wind," in *Proc. 48th IEEE Conf. Decis. Control (CDC) Held Jointly 28th Chin. Control Conf.*, Dec. 2009, pp. 776–781.
[24] S. Kim, H. Cho, and D. Jung, "Robust path following control via command-filtered backstepping scheme," *Int. J. Aeronaut. Space Sci.*, vol. 22, no. 5, pp. 1141–1153, Oct. 2021.
[25] W.-H. Chen, D. J. Ballance, P. J. Gawthrop, and J. O'Reilly, "A nonlinear disturbance observer for robotic manipulators," *IEEE Trans. Ind. Electron.*, vol. 47, no. 4, pp. 932–938, Aug. 2000.
[26] H. K. Khalil, *Nonlinear Systems*, 3rd ed. Upper Saddle River, NJ, USA: Prentice-Hall, 2002.
[27] D. Jung and P. Tsiotras, "Bank-to-turn control for a small UAV using backstepping and parameter adaptation," *IFAC Proc. Volumes*, vol. 41, no. 2, pp. 4406–4411, 2008.
[28] R. W. Beard and T. W. McLain, *Small Unmanned Aircraft: Theory and Practice*. Princeton, NJ, USA: Princeton Univ. Press, 2012.
[29] D. Kang, S. Kim, and D. Jung, "Real-time validation of formation control for fixed-wing UAVs using multi hardware-in-the-loop simulation," in *Proc. IEEE 15th Int. Conf. Control Autom. (ICCA)*, Jul. 2019, pp. 590–595.

SUHYEON KIM received the master's degree from Korea Aerospace University (KAU), Goyang-si, South Korea, in 2020, where he is currently pursuing the Ph.D. degree. His research interests include the fields of the formation flight and collision avoidance of multiple fixed-wing UAVs.

HYEONGJUN CHO received the bachelor's degree from Korea Aerospace University (KAU), Goyang-si, South Korea, in 2020, where he is currently pursuing the master's degree. His research interests include the fields of the target detection and tracking of gimbal camera.

DONGWON JUNG (Member, IEEE) received the B.S. and M.S. degrees in aerospace engineering from Seoul National University, Republic of Korea, in 1998 and 2000, respectively, and the Ph.D. degree in aerospace engineering from the Georgia Institute of Technology, Atlanta, GA, USA, in 2007. He is currently an Associate Professor with the Department of Smart Drone Convergence, Korea Aerospace University. From 2010 to 2014, he was worked at the Korea Aerospace Research Institute (KARI) as a Senior Researcher in the Division of Korea Space Launch Vehicle-2 Research and Development Program Office. His research interests include design and development of avionics systems for unmanned aerial vehicles, nonlinear guidance and trajectory optimization for autonomous vehicles, path/motion planning for multiple unmanned agents, hybrid estimation using vision, and inertial sensors.